Available online at www.sciencedirect.com
SCIENCE DIRECT®
Journal of Computational Physics 188 (2003) 281–295
JOURNAL OF COMPUTATIONAL PHYSICS
www.elsevier.com/locate/jcp

Calculation of shear stresses in the Fourier–Galerkin formulation of turbulent channel flows: projection, the Dirichlet filter and conservation ☆

Thomas J.R. Hughes [a,1], Assad A. Oberai [b,*,2]

[a] *The University of Texas at Austin, 201 East 24th Street, ACES 6.412, 1 University Station C0200, Austin, TX 78712-0027, USA*
[b] *Department of Aerospace and Mechanical Engineering, Boston University, 110 Cummington Street, Boston, MA 02215, USA*

Received 4 September 2002; received in revised form 22 January 2003; accepted 7 March 2003

Abstract

We consider turbulent channel flows computed with DNS and LES employing a Fourier–Galerkin method. We show that the balance of total mean shear stress, a measure of conservation of the numerical method, is satisfied only weakly (i.e., in an integral sense), rather than strongly (i.e., pointwise). A study of filters induced by projectors reveals that a certain filter, the *Dirichlet filter*, provides a tool for extracting shear stresses that are strongly conservative. Numerical results support the theory and demonstrate that spurious oscillations, present in the unfiltered stresses, are also suppressed.

1. Introduction

We consider turbulent channel flows calculated by direct numerical simulation (DNS) and large eddy simulation (LES) with a Fourier–Galerkin formulation. We investigate the behavior of the mean shear stresses as a pointwise function of the wall-normal coordinate. The mean shear stresses, namely, the Reynolds stress, viscous stress, and subgrid-scale stress, are physically interesting, and the residual of the shear stress balance is an indication of the satisfaction, or lack of satisfaction, of streamwise momentum conservation, which is viewed as an important measure of the veracity and accuracy of the approach. Our past experiences computing mean shear stresses reveal that they can behave anomalously in otherwise

☆ Research partially supported by NASA Ames Research Center Cooperative Agreement No. NCC 2-5363, Grant No. NAG2-1604, and ONR Grant Nos. N00014-99-1-0122, N00014-02-1-0425, and N00014-03-1-0263.
* Corresponding author. Tel.: +1-617-353-7381; fax: +1-617-353-5866.
E-mail address: oberai@bu.edu (A.A. Oberai).
[1] Professor of Aerospace Engineering and Engineering Mechanics, and Computational and Applied Mathematics Chair III.
[2] Assistant Professor.

0021-9991/03/$ - see front matter
doi:10.1016/S0021-9991(03)00167-0

accurately computed flows. In particular, spurious oscillations and violations of conservation may be observed. In order to better understand this phenomenon and identify possible remedies we observe that the total mean shear stress balance in the Fourier–Galerkin formulation is only satisfied weakly (i.e., in an integral sense), rather than strongly (i.e., pointwise), as for the exact solution. Because higher wave-number components are uncontrolled by the weak satisfaction of the total shear stress balance, oscillations and violations of conservation are not precluded. This appears to be the source of the problem. It is obvious that some type of filtering is capable of removing the high wave-number oscillations, but there is no guarantee the filtered quantity will achieve conservation. Our goal is to determine a filter which simultaneously removes oscillations and attains conservation strongly. In pursuit of this end, we briefly review least-squares approximation, the associated projection operator, and the induced filter, in terms of an undefined basis. In order to identify an appropriate basis, we look to the weak form of the conservation law. We find that a basis which removes high wave-number components and guarantees pointwise conservation ab initio, is given by the wall-normal direction derivative of the basis functions used to represent the zero wave-number component of the streamwise velocity. The corresponding projection operator is the classical *Dirichlet projector* and we dub the induced filter the *Dirichlet filter*.

We then perform numerical calculations to test the theoretical predictions. We calculate an equilibrium turbulent channel flow at a Reynolds number of 395 based on friction velocity and half channel width, with a coarse DNS and an LES employing the dynamic Smagorinsky model. The results show the unfiltered shear stresses exhibit oscillations and violate conservation, whereas the Dirichlet-filtered shear stresses confirm the theoretical predictions in that the spurious oscillations are absent and conservation is attained pointwise.

The ideas used to derive the results obtained herein are more general than the particular case considered. Variational methods, such as the Fourier–Galerkin method, often satisfy conservation laws only weakly. Analysis can reveal certain projected quantities which satisfy conservation strongly and, at the same time, exhibit higher-order accuracy. Illustrations of these concepts are contained in [1,2]. See also references therein for further elaboration. The conclusion that may be drawn from these and the present work is that there is often an optimal way to compute certain functionals of a solution. Careful analysis of the numerical method employed is an essential ingredient in achieving this objective.

An outline of the paper follows: In Section 2 we state the problem considered and recall the balance of mean shear stresses. In Section 3 we review relevant aspects of the numerical method. We then review projections, induced filters, and their roles in attaining conservation. This development leads to the identification of the Dirichlet filter as the appropriate theoretical tool. In Section 4 we present numerical results and in Section 5 we draw conclusions.

2. Theory

We consider a rectangular channel $\Omega = [0, L_x] \times [-\delta, \delta] \times [0, L_z] \subset \mathbb{R}^3$. The coordinate directions x, y, z, following the usual convention, are aligned with the streamwise, wall-normal, and spanwise directions, respectively. The velocity components are likewise denoted $\boldsymbol{u} = (u, v, w)$. The objective is to solve the incompressible, isothermal, Navier–Stokes equations in Ω, viz.,

$$\frac{\partial \boldsymbol{u}}{\partial t} = -\nabla p + \boldsymbol{H} + \nu \Delta \boldsymbol{u} + \boldsymbol{e}_x, \tag{1}$$

$$\nabla \cdot \boldsymbol{u} = 0, \tag{2}$$

where t denotes time, $\boldsymbol{H} = \boldsymbol{u} \times \boldsymbol{\omega}$, $\boldsymbol{\omega} = \nabla \times \boldsymbol{u}$ (the vorticity), Δ denotes the Laplacian, $\boldsymbol{e}_x$ is the unit vector in the x-direction, and ν is the kinematic viscosity. $Re_\tau = u_\tau \delta / \nu$ is the Reynolds number based on the friction velocity, $u_\tau = \sqrt{\tau/\rho}$, in which ρ is density and τ is the wall shear. The boundary conditions are periodic in

the x- and z-directions, and no-slip at $y = \pm\delta$. Note that the flow is driven by a prescribed unit pressure gradient in the minus x-direction. The problem configuration is schematically illustrated in Fig. 1.

By virtue of periodicity in x and z, the velocity may be written in terms of the following Fourier series:

$$\boldsymbol{u}(x,y,z,t) = \sum_{k_x}\sum_{k_z} \hat{\boldsymbol{u}}_{\boldsymbol{k}}(y,t)\mathrm{e}^{\mathrm{i}k_x x}\mathrm{e}^{\mathrm{i}k_z z}, \tag{3}$$

where $\boldsymbol{k} = (k_x, k_y)$ is the wave vector. We are interested in properties of the mean flow and so we introduce the following mean value operators:

$$[\cdot] = \frac{1}{L_x L_z}\int_0^{L_x}\int_0^{L_z} \mathrm{d}z\,\mathrm{d}x, \tag{4}$$

$$\langle\cdot\rangle = \frac{1}{T}\int_0^{T} \mathrm{d}t. \tag{5}$$

Application of $[\cdot]$ to the streamwise component of (1) results in

$$\frac{\partial U}{\partial t}(y,t) = \frac{\partial}{\partial y}\left(-\sum_{k_x}\sum_{k_z} \hat{u}_{\boldsymbol{k}}(y,t)\hat{v}_{-\boldsymbol{k}}(y,t) + \nu\frac{\partial U}{\partial y}(y,t) + y\right), \tag{6}$$

where we have introduced the notation $U = \hat{u}_{\boldsymbol{0}}$. Application of $\langle\cdot\rangle$ to (6) yields

$$\frac{U(y,T) - U(y,0)}{T} = \frac{d}{\mathrm{d}y}\left(-\left\langle \sum_{k_x}\sum_{k_z} \hat{u}_{\boldsymbol{k}}\hat{v}_{-\boldsymbol{k}}\right\rangle(y) + \nu\frac{\mathrm{d}\langle U\rangle}{\mathrm{d}y}(y) + y\right). \tag{7}$$

For T sufficiently large, we expect the left-hand side to become negligible. We also assume skew-symmetry with respect to y for the averaged quantities. These assumptions lead to the following first integral, or *conservation law*, expressing the balance of shear stresses

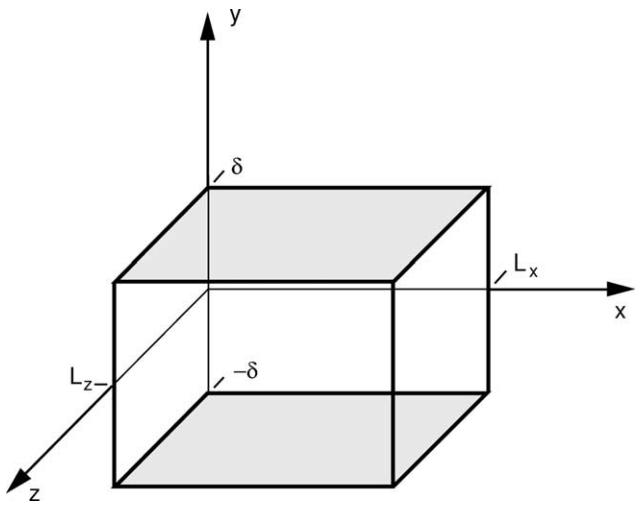

Fig. 1. Problem setup for the channel flow.

$$0 = -\left\langle \sum_{k_x} \sum_{k_z} \hat{u}_{\boldsymbol{k}} \hat{v}_{-\boldsymbol{k}} \right\rangle (y) + \nu \frac{\mathrm{d}\langle U \rangle}{\mathrm{d}y}(y) + y \quad \forall y \in [-\delta, +\delta]. \tag{8}$$

The first term in (8) is the *Reynolds shear stress* and the second is the *viscous shear stress*.

3. Discrete approximation

In the discrete approximation, the number of terms in the Fourier series is taken to be finite, say N_x and N_z for the x- and z-directions, and the Fourier coefficients are expanded in terms of basis functions in y. For example, we write

$$U^h(y,t) = \sum_{n=0}^{N_y-3} r_n(y) U_n(t), \tag{9}$$

where the superposed h is used to differentiate the approximate solution, U^h, from the exact solution, U. An example of a basis $\{r_n\}_{n=0}^{n=N_y-3}$ is given by

$$r_n(y) = \left[1 - \left(\frac{y}{\delta}\right)^2\right] P_n\left(\frac{y}{\delta}\right), \tag{10}$$

where P_n is the Legendre polynomial of order n (see [3]). Note that each r_n satisfies the no-slip boundary conditions. This basis has been introduced by Lopez and Moser [4] and results for it are reported upon in [5]. The approach is based on earlier work of Moser et al. [6] and Kim et al. [7], and the reader is referred to these works for further details. The discrete approximation of (6) employs Galerkin's method, in which the residual of (6) is orthogonalized with respect to $\{r_n\}_{n=0}^{n=N_y-3}$, viz.,

$$0 = \int_{-\delta}^{\delta} r_m(y) \left(\frac{\partial U^h}{\partial t}(y,t) - \frac{\partial}{\partial y} \left(- \sum_{k_x} \sum_{k_z} \hat{u}^h_{\boldsymbol{k}}(y,t) \hat{v}^h_{-\boldsymbol{k}}(y,t) + \nu \frac{\partial U^h}{\partial y}(y,t) + y \right) \right) \mathrm{d}y,$$
$$m = 0, 1, \ldots, N_y - 3, \tag{11}$$

where $\hat{u}^h_{\boldsymbol{k}}$ and $\hat{v}^h_{\boldsymbol{k}}$ are discrete approximations of $\hat{u}_{\boldsymbol{k}}$ and $\hat{v}_{\boldsymbol{k}}$, respectively. Application of the mean value operator $\langle \cdot \rangle$ to (11) yields

$$\int_{-\delta}^{\delta} r_m(y) \left(\frac{U^h(y,T) - U^h(y,0)}{T} \right) \mathrm{d}y = \int_{-\delta}^{\delta} r_m(y) \left(\frac{\mathrm{d}}{\mathrm{d}y} \left(- \left\langle \sum_{k_x} \sum_{k_z} \hat{u}^h_{\boldsymbol{k}} \hat{v}^h_{-\boldsymbol{k}} \right\rangle (y) + \nu \frac{\mathrm{d}\langle U^h \rangle}{\mathrm{d}y}(y) + y \right) \right) \mathrm{d}y,$$
$$m = 0, 1, \ldots, N_y - 3. \tag{12}$$

As in the continuous case, we expect the left-hand side becomes negligible for sufficiently large T. Assuming this to be the case and integrating-by-parts results in

$$0 = \int_{-\delta}^{\delta} \frac{\mathrm{d}r_m}{\mathrm{d}y}(y) \left(- \left\langle \sum_{k_x} \sum_{k_z} \hat{u}^h_{\boldsymbol{k}} \hat{v}^h_{-\boldsymbol{k}} \right\rangle (y) + \nu \frac{\mathrm{d}\langle U^h \rangle}{\mathrm{d}y}(y) + y \right) \mathrm{d}y, \quad m = 0, 1, \ldots, N_y - 3, \tag{13}$$

where we have used the fact that the basis functions satisfy the no-slip boundary condition, that is, $r_m(\pm\delta) = 0$, $m = 0, 1, \ldots, N_y - 3$. This is the discrete analog of (8), but note, in contrast to the continuous case where the conservation law is satisfied *strongly* as a function of $y \in [-\delta, \delta]$, here it is satisfied *weakly*, in an integral sense. This has implications with respect to the way we calculate shear stresses.

Remarks

(1) In practice, a time-integration algorithm is used to discretize time. The deductions made place restrictions on the time-integration scheme, but they are typically satisfied by commonly used methods. It is sufficient that the time-integration scheme discretizes in such a way that (12) can be derived from the time-discretized version of (11). This means that the summation over time steps produces a simple difference quotient form of the time derivative (see (11)).

(2) The results obtained are applicable to cases in which functions other than Fourier modes and modified Legendre polynomials are used. However it is important that the wall-normal functions vanish at the walls.

3.1. Projection

Let $\mathscr{V} = L_2(-\delta,\delta) = \{f \,|\, f : (-\delta,\delta) \to \mathbb{R}, \int_{-\delta}^{\delta} (f(y))^2 \,\mathrm{d}y < \infty\}$. Consider a finite-dimensional subspace of $\mathscr{V}$, denoted by $\tilde{\mathscr{V}}$, spanned by a basis $\{\phi_n\}_{n=0}^{N}$. Let $\tilde{\boldsymbol{\Pi}} : \mathscr{V} \to \tilde{\mathscr{V}}$ denote the L_2-projection operator onto $\tilde{\mathscr{V}}$. $\tilde{\boldsymbol{\Pi}}$ is characterized by the variational problem: Given $f \in \mathscr{V}$, find $\tilde{f} \in \tilde{\mathscr{V}}$ such that the least-squares potential

$$P(\tilde{f}) = \frac{1}{2}\int_{-\delta}^{\delta} (\tilde{f}(y) - f(y))^2 \mathrm{d}y, \tag{14}$$

is minimized, where

$$\tilde{f}(y) = \sum_{n=0}^{N} \phi_n(y)\tilde{f}_n = \boldsymbol{\phi}(y)\cdot\tilde{\boldsymbol{f}} \tag{15}$$

in which $\boldsymbol{\phi} = (\phi_0, \phi_1, \ldots, \phi_N)^{\mathrm{T}}$ and $\tilde{\boldsymbol{f}} = (\tilde{f}_0, \tilde{f}_1, \ldots, \tilde{f}_N)^{\mathrm{T}}$. The solution of the variational problem is obtained by solving the linear system

$$\sum_{n=0}^{N} \int_{-\delta}^{\delta} \phi_m(y)\phi_n(y)\,\mathrm{d}y\tilde{f}_n = \int_{-\delta}^{\delta} \phi_m(y) f(y)\mathrm{d}y, \quad m = 0, 1, \ldots, N. \tag{16}$$

In matrix notation this can be written as

$$\boldsymbol{M}\tilde{\boldsymbol{f}} = \boldsymbol{f}\,, \tag{17}$$

where

$$\boldsymbol{M} = \int_{-\delta}^{\delta} \boldsymbol{\phi}(y)\otimes\boldsymbol{\phi}(y)\mathrm{d}y, \tag{18}$$

$$\boldsymbol{f} = \int_{-\delta}^{\delta} \boldsymbol{\phi}(y) f(y)\mathrm{d}y. \tag{19}$$

In (18), $\otimes$ is the tensor, or outer, product, and $\boldsymbol{M}$ is referred to as the *Gram*, or *mass*, *matrix*. Note from (16), that if $f \in \mathscr{V}$ is orthogonal to the basis of $\tilde{\mathscr{V}}$, then $\boldsymbol{f} = \boldsymbol{0}$, and $\tilde{f} = \tilde{\boldsymbol{\Pi}} f = 0$.

3.2. Induced filter

The projector $\tilde{\boldsymbol{\Pi}}$ induces a filter defined by (see [8,9])

$$\tilde{f} = \tilde{\boldsymbol{\Pi}} f = g \bigstar f, \tag{20}$$

$$\tilde{f}(y) = \int_{-\delta}^{\delta} g(y,y')f(y')\mathrm{d}y', \tag{21}$$

where g, the kernel, is given by

$$g(y,y') = \boldsymbol{\phi}(y)\cdot\boldsymbol{M}^{-1}\boldsymbol{\phi}(y'). \tag{22}$$

This can be seen from the following calculation:

$$\begin{aligned}\tilde{f}(y) &= \boldsymbol{\phi}(y)\cdot\tilde{\boldsymbol{f}} \quad \text{(by (15))}\\ &= \boldsymbol{\phi}(y)\cdot\boldsymbol{M}^{-1}\boldsymbol{f} \quad \text{(by (17))}\\ &= \boldsymbol{\phi}(y)\cdot\boldsymbol{M}^{-1}\int_{-\delta}^{\delta}\boldsymbol{\phi}(y')f(y')\mathrm{d}y' \quad \text{(by (19))}\\ &= \int_{-\delta}^{\delta}\boldsymbol{\phi}(y)\cdot\boldsymbol{M}^{-1}\boldsymbol{\phi}(y')f(y')\mathrm{d}y'.\end{aligned} \tag{23}$$

Due to the symmetry of $\boldsymbol{M}$, $g(y,y') = g(y',y)$. However, in general, g will be *inhomogeneous*.

3.3. Discrete conservation law

Define $f \in \mathscr{V}$ by

$$f = -\left\langle \sum_{k_x}\sum_{k_z}\hat{\boldsymbol{u}}^h_{\boldsymbol{k}}\hat{v}^h_{-\boldsymbol{k}}\right\rangle + \nu\frac{\mathrm{d}\langle U^h\rangle}{\mathrm{d}y} + id, \tag{24}$$

where id is the identity operator, i.e., $id(y) = y$. Specify $\tilde{\mathscr{V}}$ in the following way:

$$\tilde{\mathscr{V}} = \mathrm{span}\left\{\frac{\mathrm{d}r_n}{\mathrm{d}y}\right\}_{n=0}^{N_y-3}. \tag{25}$$

In the previous developments this amounts to setting $\phi_n = \mathrm{d}r_n/\mathrm{d}y, n = 0,1,\ldots,N = N_y - 3$. Then, from (13), we see that $f \in \mathscr{V}$ is orthogonal to $\tilde{\mathscr{V}}$. Consequently, $\tilde{f} = \tilde{\Pi}f = 0$. By the linearity of $\tilde{\Pi}$, it follows that

$$0 = \tilde{f} = -\tilde{\Pi}\left\langle \sum_{k_x}\sum_{k_z}\hat{\boldsymbol{u}}^h_{\boldsymbol{k}}\hat{v}^h_{-\boldsymbol{k}}\right\rangle + \tilde{\Pi}\nu\frac{\mathrm{d}\langle U^h\rangle}{\mathrm{d}y} + \tilde{\Pi}\,id. \tag{26}$$

Eq. (26) says that the L_2-projections of the numerically calculated Reynolds and viscous shear stresses, onto the space of y-derivatives of the basis functions used in the expansion of U^h, satisfy a pointwise conservation law identical to that of the exact solution (cf. (8)).

Remarks

(1) The filter induced by L_2-projection onto $\tilde{\mathscr{V}}$, given by (25), is defined by

$$g(y,y') = \frac{\mathrm{d}\boldsymbol{r}}{\mathrm{d}y}(y)\cdot\boldsymbol{K}^{-1}\frac{\mathrm{d}\boldsymbol{r}}{\mathrm{d}y}(y'), \tag{27}$$

where $\boldsymbol{r} = (r_0, r_1, \ldots, r_{N_y-3})^{\mathrm{T}}$, and

$$\boldsymbol{K} = \int_{-\delta}^{\delta} \frac{\mathrm{d}\boldsymbol{r}}{\mathrm{d}y}(y) \otimes \frac{\mathrm{d}\boldsymbol{r}}{\mathrm{d}y}(y)\,\mathrm{d}y \tag{28}$$

which is referred to as the *Dirichlet*, or *stiffness*, *matrix*. $\tilde{\Pi}$ is called the *Dirichlet projector* in this case, and (27) is the kernel defining the *Dirichlet filter*.

(2) If a subgrid-scale stress model is included, the results need to be generalized as follows. Let $\tilde{T}^h_{yx\mathbf{0}}(y,t)$ denote the numerically computed Fourier coefficient of the zero wave-vector y,x-component of the subgrid-scale shear stress. Then

$$f = -\left\langle \sum_{k_x} \sum_{k_z} \hat{u}^h_{\boldsymbol{k}} \hat{v}^h_{-\boldsymbol{k}} \right\rangle + \tilde{T}^h_{yx\mathbf{0}} + \nu \frac{\mathrm{d}\langle U^h \rangle}{\mathrm{d}y} + id \tag{29}$$

and

$$0 = \tilde{f} = -\tilde{\Pi}\left\langle \sum_{k_x} \sum_{k_z} \hat{u}^h_{\boldsymbol{k}} \hat{v}^h_{-\boldsymbol{k}} \right\rangle + \tilde{\Pi}\tilde{T}^h_{yx\mathbf{0}} + \tilde{\Pi}\nu \frac{\mathrm{d}\langle U^h \rangle}{\mathrm{d}y} + \tilde{\Pi}\, id. \tag{30}$$

(3) In the case of the basis defined by (10)

$$\frac{\mathrm{d}r_0}{\mathrm{d}y}(y) = -2yP_0/\delta^2 \tag{31}$$

in which P_0 is a constant. Consequently, this basis contains the monomial y. As a result $\tilde{\Pi}\, id = id$, and thus the projected Reynolds, model and viscous shear stresses in (30) will sum *exactly* to $-y$.

(4) The functions f and $\tilde{f}$ given by (24), (26), (29) and (30) may be viewed as *residuals* of the balance of total shear stress and thus may be used as measures of error in numerical calculations. This is the view taken in the following section.

4. Numerical results

We consider an $Re_\tau = 395$ equilibrium channel flow and employ the method described previously using the modified Legendre basis. A resolution of $N_x = N_y = N_z = 32$ is used, and $L_x = 2\pi$, $\delta = 1$, and $L_z = 4\pi/3$.

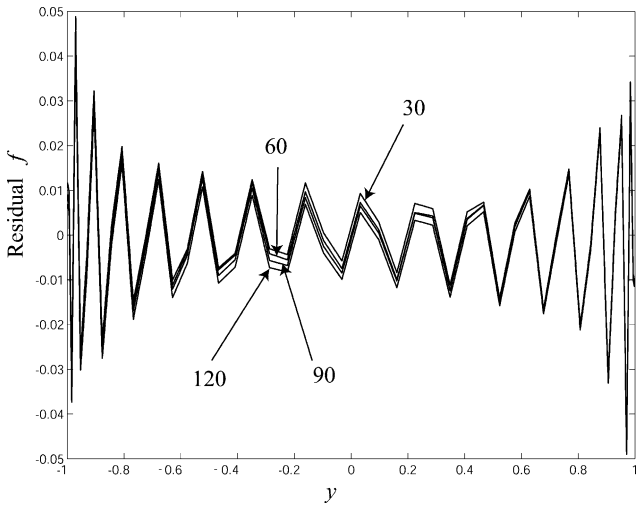

Fig. 2. Unfiltered total shear stress residual at various times (coarse DNS).

See [5] for additional details. We compare unfiltered and Dirichlet-filtered quantities. We study the pointwise convergence of the residuals f and $\tilde{f}$ with time, f versus $\tilde{f}$ at particular times, the L_2-error convergence in f and $\tilde{f}$ with time, and the budgets of f and $\tilde{f}$ at specific times. The L_2-residual errors are defined by

$$e_f = \left(\int_{-\delta}^{\delta} (f(y))^2 \, \mathrm{d}y \right)^{1/2}, \tag{32}$$

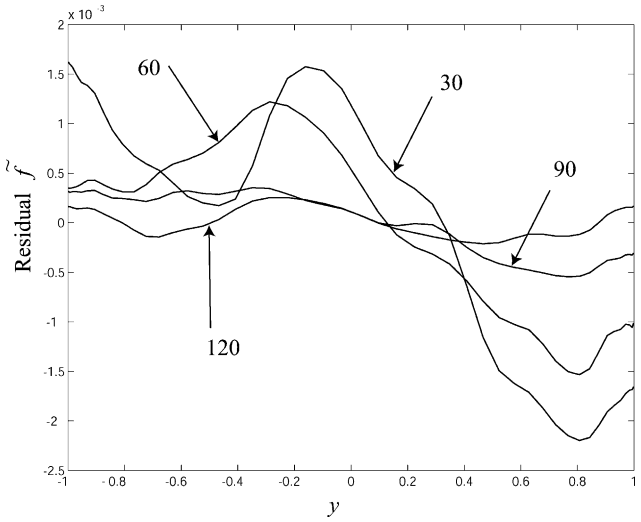

Fig. 3. Dirichlet-filtered total shear stress residual at various times (coarse DNS).

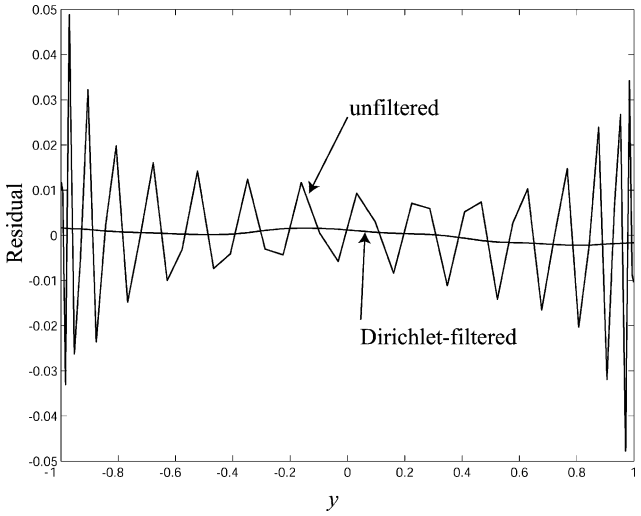

Fig. 4. Comparison of unfiltered and Dirichlet-filtered total shear stress residual at $t = 30$ (coarse DNS).

$$e_{\tilde{f}} = \left(\int_{-\delta}^{\delta} (\tilde{f}(y))^2 \, \mathrm{d}y \right)^{1/2}. \tag{33}$$

4.1. Coarse DNS

The mean centerline velocity is approximately 18.3. Thus it takes 0.34 time units for a centerline fluid particle to flow through the domain. This calculation was run for 120 time units which is about 353 flow-through times. Figs. 2 and 3 show the convergence of f and $\tilde{f}$, defined by (24) and (26), respectively. Note from Fig. 2 that the unfiltered case exhibits significant oscillations which do not diminish with time,

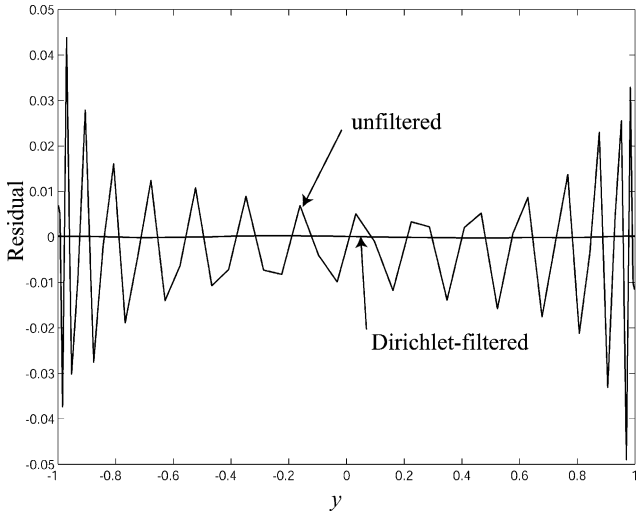

Fig. 5. Comparison of unfiltered and Dirichlet-filtered total shear stress residual at $t = 120$ (coarse DNS).

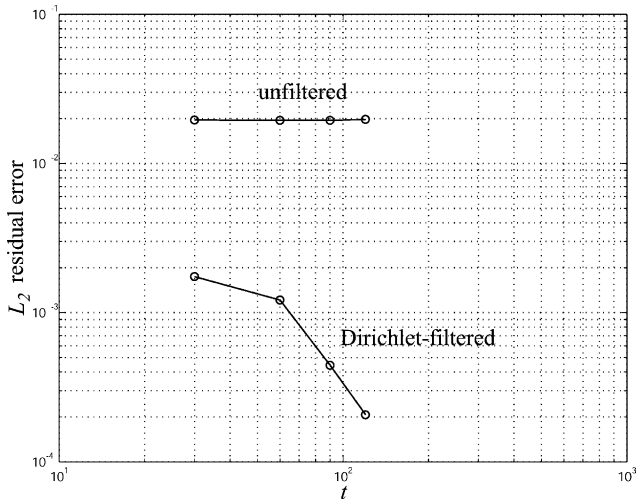

Fig. 6. L_2-errors in unfiltered and Dirichlet-filtered total shear stress residuals versus time (coarse DNS).

whereas the Dirichlet-filtered case in Fig. 3 is converging to zero. Note also that the scale in Fig. 3 is about an order of magnitude smaller than Fig. 2 and thus $\tilde{f}$ is actually much smaller than f. This can be seen by comparing f and $\tilde{f}$ at $t = 30$ and 120, in Figs. 4 and 5, respectively. A comparison of the L_2-error in Fig. 6 clearly shows lack of convergence of the unfiltered case and convergence of the Dirichlet-filtered case of approximate $O(t^{-1})$. Finally, budgets of f and $\tilde{f}$ at $t = 120$ are presented in Figs. 7 and 8. In the unfiltered case the oscillations are seen to emanate from the Reynolds shear stress. (A comparison of the Reynolds stress with the DNS benchmark solution of Moser et al. [10] is presented in Fig. 31 of [5] . Despite the coarseness of our simulation, the results compare very well.)

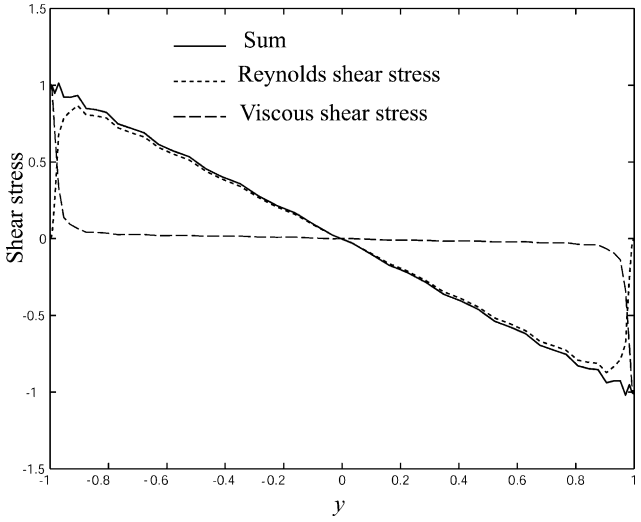

Fig. 7. Unfiltered shear stress budget at $t = 120$ (coarse DNS).

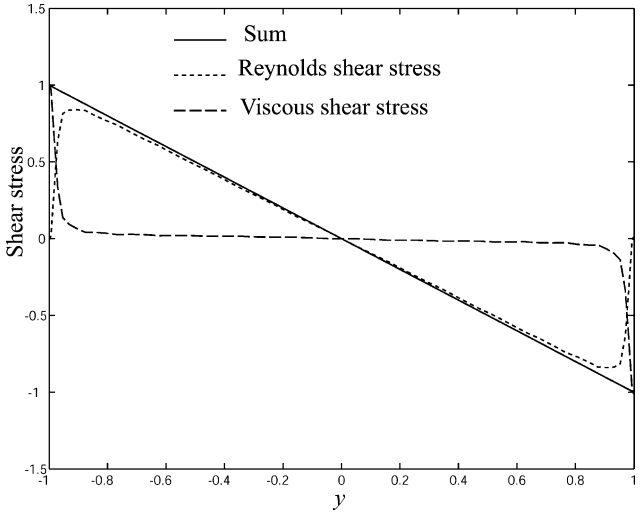

Fig. 8. Dirichlet-filtered shear stress budget at $t = 120$ (coarse DNS).

4.2. Dynamic model

A similar study was undertaken for the dynamic Smagorinsky model (see [11–14]). Implementational details may be found in [5]. The mean centerline velocity is approximately 20.9. Thus it takes 0.3 time units for a centerline fluid particle to flow through the domain. The calculation was run for 116 time units, which is about 387 flow-through times. Figs. 9 and 10 show the convergence of f and $\tilde{f}$ defined by (29) and (30), respectively. The results are similar to the coarse DNS case in that the unfiltered residual fails to converge whereas the Dirichlet-filtered residual does converge. Note again that the scale of Fig. 10 is about an order of magnitude smaller than Fig. 9, and likewise $\tilde{f}$ is much smaller than f. This can be seen better by

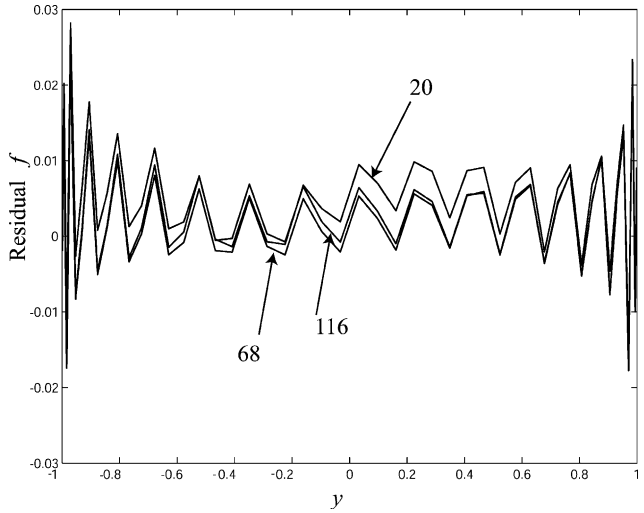

Fig. 9. Unfiltered total shear stress residual at various times (dynamic Smagorinsky model).

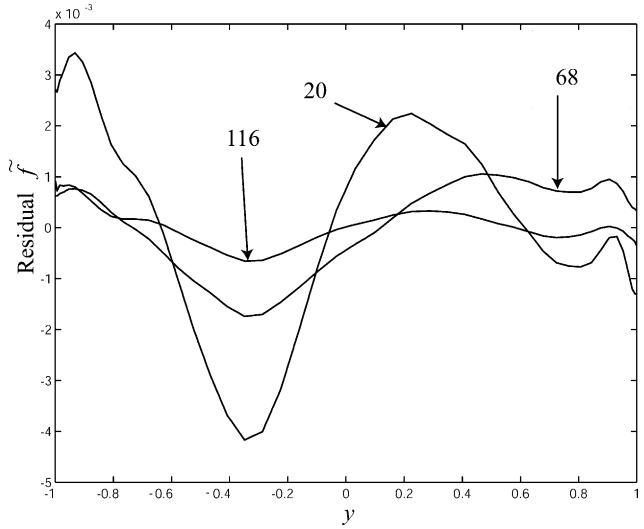

Fig. 10. Dirichlet-filtered total shear stress residual at various times (dynamic Smagorinsky model).

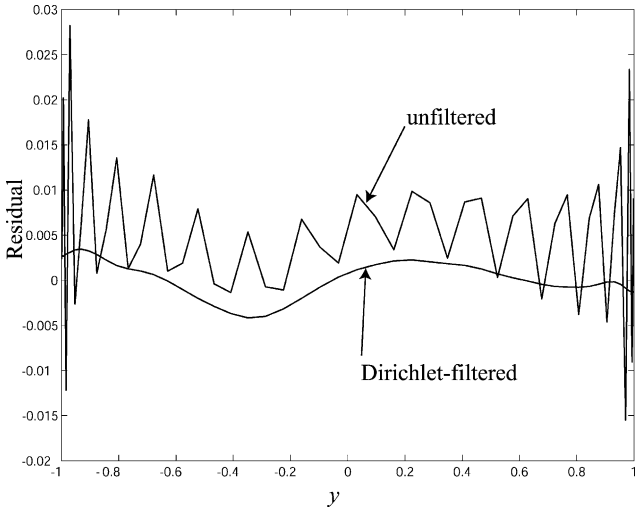

Fig. 11. Comparison of unfiltered and Dirichlet-filtered total shear stress residual at $t = 20$ (dynamic Smagorinsky model).

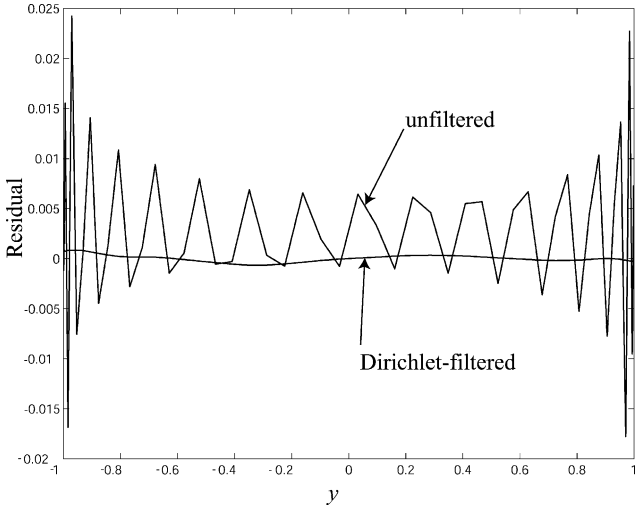

Fig. 12. Comparison of unfiltered and Dirichlet-filtered total shear stress residual at $t = 116$ (dynamic Smagorinsky model).

comparisons of f and $\tilde{f}$ at $t = 20$ and 116 in Figs. 11 and 12, respectively. Note that in Figs. 11 and 12, in addition to a highly oscillatory component of error, there is a very low mode component as well, unlike the coarse DNS case. This mode is approximately constant and might not be removed by increased resolution. The L_2-errors are presented in Fig. 13. The unfiltered case fails to converge and the convergence of the filtered case is roughly $O(t^{-1})$. Finally the budgets of f and $\tilde{f}$ at $t = 116$ are presented in Figs. 14 and 15, respectively. As in the coarse DNS case, oscillations are visible in the unfiltered case. (An accuracy assessment of the Reynolds stress, model included, with the DNS benchmark of Moser, et al. [10] is presented in Fig. 31 of [5]. Again, the accuracy is quite good.)

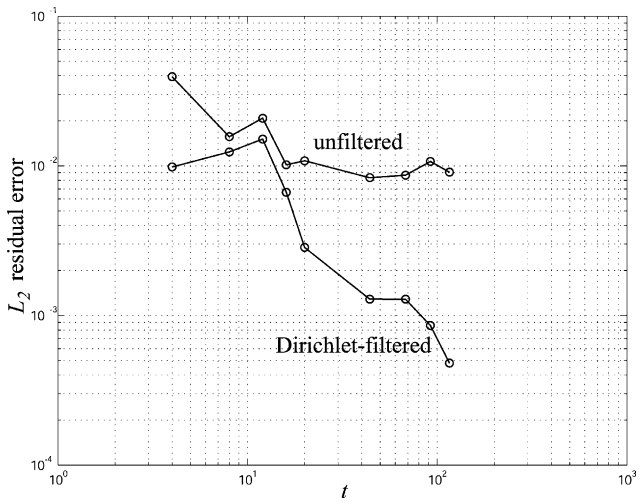

Fig. 13. L_2-errors in unfiltered and Dirichlet-filtered total shear stress residuals versus time (dynamic Smagorinsky model).

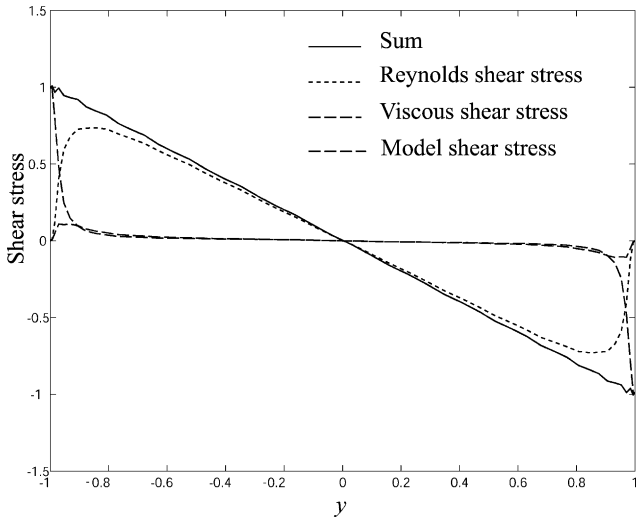

Fig. 14. Unfiltered shear stress budget at $t = 116$ (dynamic Smagorinsky model).

5. Conclusions

We have examined the Fourier–Galerkin formulation of turbulent channel flows and shown that the Dirichlet-filtered mean shear stresses satisfy the balance of total shear stress, a measure of conservation, pointwise, even though the unfiltered stresses only satisfy conservation in a weak, integral sense. The Dirichlet filter is thus identified as the appropriate tool for computing the shear stress budget. The theoretical ideas are supported by numerical calculations of a coarse DNS and an LES employing the dynamic Smagorinsky model.

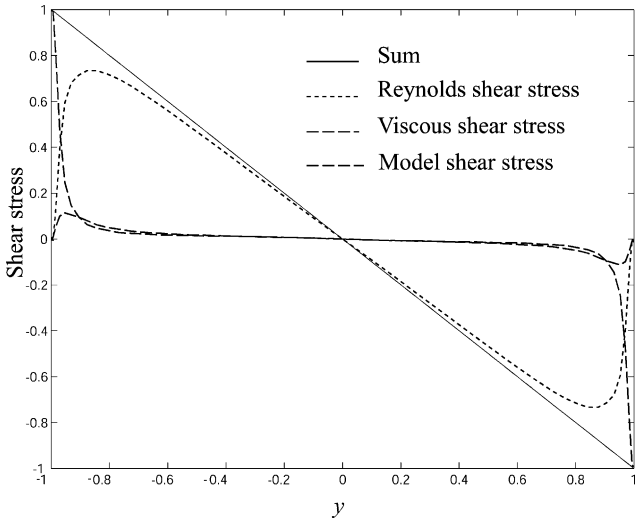

Fig. 15. Dirichlet-filtered shear stress budget at $t = 116$ (dynamic Smagorinsky model).

The ideas presented are more general than the specific application. They represent ways of extricating information from calculations that simultaneously are higher-order accurate and precisely attain conservation.

Acknowledgements

We wish to express our sincere appreciation to V. Lopez and R. Moser who provided us with their channel flow code which served as the basis of the numerical calculations reported herein.

References

[1] T.J.R. Hughes, G. Engel, L. Mazzei, M.G. Larson, The continuous Galerkin method is locally conservative, Journal of Computational Physics 163 (2000) 467–488.
[2] F. Brezzi, T.J.R. Hughes, E. Süli, Variational approximation of flux in conforming finite element methods for elliptic partial differential equations: a model problem, Atti dell'Accademia Nazionale dei Lincei 12 (2002) 167–183.
[3] C. Canuto, M.Y. Hussaini, A. Quarteroni, T.A. Zang, Spectral Methods in Fluid Dynamics, Springer, Berlin, Heidelberg, 1988.
[4] V. Lopez and R.D. Moser, Private communication, 1999.
[5] T.J.R. Hughes, A.A. Oberai, L. Mazzei, Large eddy simulation of turbulent channel flows by the variational multiscale method, Physics of Fluids 13 (6) (2001) 1784–1799.
[6] R.D. Moser, P. Moin, A. Leonard, A Spectral numerical method for the Navier–Stokes equations with applications to Taylor–Couette flow, Journal of Computational Physics 52 (1983) 524–544.
[7] J. Kim, P. Moin, R.D. Moser, Turbulence statistics in fully developed channel flow at low reynolds number, Journal of Fluid Mechanics 177 (1987) 133–166.
[8] P. Sagaut, Large Eddy Simulation for Incompressible Flows, Springer, Berlin, 2001.
[9] S.B. Pope, Turbulent Flows, Cambridge University Press, Cambridge, MA, 2000.
[10] R.D. Moser, J. Kim, N. Mansour, Direct numerical simulation of turbulent channel flows up to $Re_\tau = 590$, Physics of Fluids 11 (1999) 943–945.
[11] M. Germano, U. Piomelli, P. Moin, W.H. Cabot, A dynamic subgrid-scale eddy viscosity model, Physics of Fluids 3 (7) (1991) 1760–1765.

[12] S. Ghosal, T.S. Lund, P. Moin, A local dynamic model for large-eddy simulation, Technical Report, CTR Annual Research Briefs, Center for Turbulence Research, Stanford University/NASA Ames Research Center, 1992.
[13] S. Ghosal, T.S. Lund, P. Moin, K. Akselvoll, A dynamic localization model for large-eddy simulation of turbulent flows, Journal of Fluid Mechanics 286 (1995) 229–255.
[14] D.K. Lilly, A proposed modification of the Germano subgrid-scale closure method, Physics of Fluids A 4 (1992) 633–635.